ISSN: 2277-9655
Scientific Journal Impact Factor: 3.449
(ISRA), Impact Factor: 2.114

IJESRT

INTERNATIONAL JOURNAL OF ENGINEERING SCIENCES & RESEARCH TECHNOLOGY

Fabrication and Characterization of Low-Temperature Conductive Film Bonded Crystalline Silicon Solar Cells and PV Modules

Su-Wung Baek*[a,d], Kwang-Il Choi[a], Suk-Ho Lee[a], Chan-Hyuk Cheon[b], Seung-Min Hong[b], Kil-Song Lee[c], Hyun-Woo Shin[c], Yeon-Won Yang[c] ,Cheolhyun Lim*[a]

[*a]Green Energy Institute, 177, Samhyangcheon-ro, Mokpo-si, Jeollanam-do 530-400, Korea
[b]Aaron Co., Ltd, Changgok-ri, Paltan-myeon, Hwaseong-Si, Gyeonggi-do 103-022, Korea
[c]Solar Tech Co., Ltd., Suite 712, Yucheon Factopia, #196, Anyang-7 Dong, Mana-Gu, Anyang-City, Kyonggi-do 403-817, Korea
[d]Department of Chemical Engineering, Chonbuk National University, Jeonju 561-756, Korea

Abstract

Low-temperature conductive films (LT-CFs) were examined as a bonding material for fabricating a solar cell string. Morphological, mechanical, and electrical contact properties of the LT-CFs and solar cells bonded using them under various conditions were carefully evaluated. In particular, a value combining all sample bonding parameters, V_{BP} (V_{BP} = temperature (°C) × pressure (MPa) × time (h)), was introduced.On the basis of the results obtained, the parameter range was divided into three regimes: soft, moderate, and hard regime. The moderate regime was corresponded to strong bonding and low power loss. LT-CF-bonded cells in this regime showed a compression rate of 39.7–45.0 % corresponding to a reaction rate of 80–90 %, peeling strength of ~1 N/mm, and power loss of 1.2–3.3 %. Further, to analyze the effectiveness of the LT-CF process in preventing thermal stress in comparison to a conventional soldering ribbon (SR) process, the bows of LT-CF-bonded and conventional SR-bonded cells were compared. The average bow of the LT-CF-bonded cells (1.42 mm) was lower than that of the SR-bonded cells (3.15 mm), representing a bow suppression of 54.9 %

Keywords: Low-temperature conductive film; PV module; bonding; peeling strength; power loss; bow

Introduction

The conventional soldering technique for silicon photovoltaic (PV) module production using solder-coated copper ribbons (SRs) at a curing temperature of 200 °C or higher provides good mechanical and electrical contact between solar cells and ribbons. However, the need to reduce manufacturing costs has resulted in a steady reduction in the solar cell thickness. This thickness reduction has resulted in the soldering of ribbons to cells becoming a challenging step. Further, the residual thermal and mechanical stress between metal ribbons and solar cells generated during the bonding process is a critical issue for thinner cells as it results in deterioration of manufacturability, reliability, and module efficiency. Therefore, alternative techniques are required that can provide the same mechanical and electrical contact properties afforded by the conventional soldering techniques, as well as can simultaneously reduce the process temperature. Various types of low-temperature bonding techniques, including bonding solder materials and processes, have been widely investigated in the semiconductor packaging and manufacturing industry [1,2]. Among these methods, intensive research has been conducted on conductive film (CF) bonding as an alternative method to soldering [3-5]. Recently, low-temperature conductive films (LT-CFs) for use in the solar cell bonding process were introduced and commercialized [6,7]. This process not only provides significant reduction in residual thermal stress but is also environmentally friendly owing to the absence of flux and Pb. CFs consist of thermosetting epoxy resins and are filled with randomly dispersed conductive particles. The application of heat and pressure results in curing of the thermosetting epoxy resins, and this curing provides physical and mechanical adhesion between the contact surfaces. Moreover, conductive paths formed by the deformation of conductive particles provide electrical conduction inside the cured epoxy resins. Therefore, the contact properties of CFs depend on the bonding parameters and the CF material itself. In this study, we investigated the morphological changes, adhesion strength, power loss, and bow of silicon solar cells bonded under

ISSN: 2277-9655
Scientific Journal Impact Factor: 3.449
(ISRA), Impact Factor: 2.114

various conditions via the latest developed CF bonding pilot line, which is capable of bonding 700 cells/h (ARCF-700), at AARON. On the basis of the results obtained, 250-Wp PV modules bonded using LT-CFs and SRs bonded were fabricated and compared. Finally, a light-capturing ribbon (LCR) was used to enhance the module efficiency.

Materials and methods

Bonding materials

The LT-CF used in this study was a commercial product, CF-205 (Hitachi Chemical). It was inserted between a Pb-free ribbon (PFR; Sn-96.5, Ag-3.5, in at%) and a monocrystalline silicon solar cell (6 inch, 3-bus bar, 4.54 Wp) to form mechanical and electrical bonding. The thickness and width of the LT-CF were 25 µm and 1.2 mm, respectively. The LT-CF consisted of thermosetting epoxy resins in which Ni polymer particles with an average diameter of 5 µm were dispersed.

Bonding parameters

In order to optimize the bonding conditions, various parameters were examined. The bonding temperature was varied from 110 to 210 °C, and the bonding time was varied from 1 to 7 s. Further, the bonding pressure was varied from 1 to 4 MPa. Herein, the dependence of various properties of LT-CF-bonded cells and LT-CF itself on the bonding parameters is represented by the product of all parameters corresponding to the bonding of one sample, V_{BP}, has been introduced, as shown in equation 1. This quantity allows all the parameters to be displayed in a single figure and each parameter is represented using a different symbol for better understanding.

$$V_{BP}\ (Bonding\ Parameters) = Temperature\ (℃) \times Pressure\ (Mpa) \times Time\ (h) \quad (1)$$

Table 1. Bonding materials and parameters for cell and module production

Sample	Bonding process	Ribbon	Temperature (℃)	Time (s)	Pressure (MPa)
SR	Soldering	SR (60Sn 40Pb)	250	2	-
CF-PFR	LT-CF	PFR (96.5Sn 3.6Ag)	180	5	2
CF-LCR	LT-CF	LCR (99.9Ag-coated Cu)	180	5	2

Optimized bonding procedure

As shown in Fig. 1, the procedure for LT-CF bonding consists of the following steps: LT-CF placement on cells, pre-bonding, PFR placement, and final bonding.

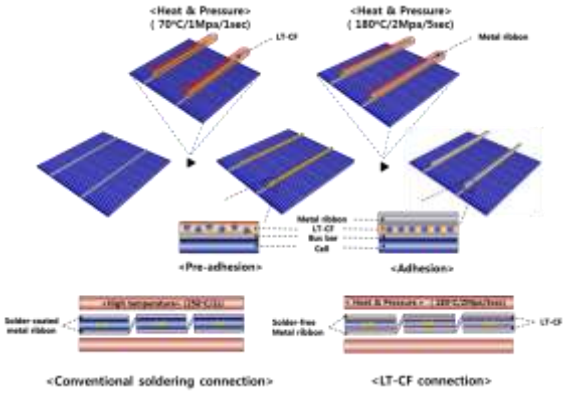

Fig. 1. Optimized bonding procedure using LT-CF

The whole procedure was automatically carried out using a pilot apparatus (ARCF-700), which is capable of interconnecting 700 cells/h. As the first step, LT-CF was placed on the solar cell and then pre-bonding was carried out under a pressure of 1 MPa and a temperature of 70 °C for a time of 1 s. The positions of the pre-bonded cell and PFR were aligned automatically.

Finally, the PFR was bonded to the cell by simultaneously applying heat and pressure. The final bonding pressure and time were 2 MPa and 5 s, respectively, while the bonding temperature was 180 °C. The bonding parameters and CF film specifications are summarized in Table 1. For comparison, a conventional soldering process was also conducted using a SR (Sn-60, Pb-40, in at%) on the same cell at a curing temperature of 250 °C for 2 s.

Modules

For comparison, three different types of 250-Wp PV modules (10 × 6 = 60 cells) were fabricated using different bonding materials and ribbons. Module SR (control sample) was fabricated by the conventional soldering process using SR. Modules CF-PFR and CF-LCR were produced by the LT-CF process but using different ribbons, namely, PFR and LCR, respectively.

Characterization

The surfaces and cross-sections of the interface between bonded cells and ribbons were observed by scanning electron microscopy (SEM, SNE-4500M). Energy-dispersive spectrometry (EDS, Bruker Nano) was used to analyze the composition of

ISSN: 2277-9655
Scientific Journal Impact Factor: 3.449
(ISRA), Impact Factor: 2.114

bonding materials. Fourier transform infrared (FT-IR) spectroscopy was used to examine the reaction rate of LT-CF. The reaction rate was calculated by comparing the two peak areas derived from an epoxy functional group at 915 cm^{-1} and an aromatic ring band at 1507 cm^{-1} [8]. To measure the adhesion strength, the 90 ° peel test was carried out. The bonded three ribbons on the cells were peeled-off, and the peel strength was measured using a peel tester (IMADA, DS2-20N) at a peeling speed of 0.7 mm/s. Power loss in the solar cell was analyzed before and after the bonding process, and power output was simulated using a flash system (McScience, Lab200) with the AAA class in spectrum. In order to study the bow in the cell due to the residual thermal stress, the deflection at the center of cell was measured before and after the soldering process. For microcrack detection, electroluminescence (EL, McScience, K5500) measurements were conducted on the modules. The electrical characteristics of the modules were evaluated using a solar module simulator (HSPV,HSM2-2LA) with the AAA class in spectrum under standard conditions.

Results and discussion

The thickness and width of LT-CF were 25 µm and 1.2 mm, respectively, and Ni polymer particles with an average diameter of 5 µm were uniformly dispersed as shown in Fig. 2(a). From this surface image, the density of the Ni particles was estimated to be ~1.84 × 10^8 pariticles·cm^{-3}. Fig. 2(b) shows the EDX analysis results for LT-CF.

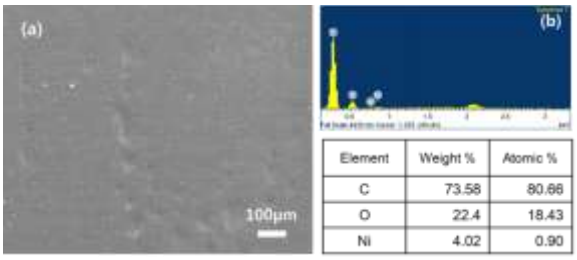

Fig. 2. Surface image of (a) LT-CF and (b) corresponding EDX analysis.

The results revealed that LT-CF was composed of 73.58 wt% C, 22.4 wt% O, and 4.02 wt% Ni. A relatively large amount of O was observed in the LT-CF sample. As the epoxy contained only 3–5 wt% O, the large O amount can be attributed to the exposure of samples in air for about 2 weeks. Such a high O amount can presumably increase the contact resistance and weaken the bonding strength of LT-CF owing to the oxidation of Ni particles [9]. Therefore, it is important to prevent the oxidation of LT-CF.

In order to clarify the morphology changes in LT-CF after the bonding process according to the bonding parameters, cross-sectional and top-view images of the interface between the bonded cells and ribbons were observed.

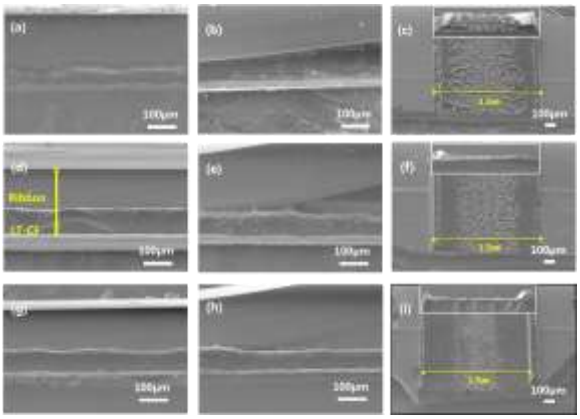

Fig. 3. Cross-sectional and top-view images of LT-CF-bonded cells assembled at various temperatures: (a)–(c) 110 ℃, (d)–(f) 180 ℃, and (g)–(i) 210 ℃ for 5 s at 2 MPa. (a), (d), (g) Cross-sectional images of outflow of LT-CF after bonding; (b), (e), (h) cross-sectional images of failure modes of LT-CF; (c), (f), (i) top-view images of LT-CF after removal of ribbon. Insets: corresponding cross-sectional images of LT-CFs.

Among the LT-CF-bonded samples prepared under various values for the parameters temperature, pressure, and time, the most representative parameter series that explained well morphology changes in LT-CFs after the bonding process was the temperature-varied samples, as shown in Fig. 3. Fig. 3(a)–(c) show the cross-sectional and top-view images of LT-CF-bonded samples prepared at 110 °C. Fig. 3(d)–(f) and (g)–(i) show the results for the samples bonded at 180 and 210 °C, respectively. For all samples, pressure and time were fixed at 2 MPa and 2 s, respectively. In particular, Fig. 3(a), (d), and (g) show the cross-sectional images of the outflow of LT-CF after bonding, and (b), (e), and (h) show the cross-sectional images depicting the failure modes of LT-CF. Fig. 3(c), (f), and (i) are top-view images showing LT-CF after the removal of the ribbon, and the insets in these figures correspond to the cross-sectional images of LT-CF samples.

As mentioned in Fig. 3(d), the original thickness of the ribbon and LT-CF were 200 and 25 µm, respectively. However, the thickness after bonding as obtained from their cross-sectional images was ~140 and 85 µm, respectively. This implies that the ribbon was buried in LT-CF, and LT-

ISSN: 2277-9655
Scientific Journal Impact Factor: 3.449
(ISRA), Impact Factor: 2.114

CF beneath the ribbon flowed out after the bonding process. Fig. 3(a), (d), and (g) show that the ribbon was buried and flowed out more as the temperature increased. Fig. 3(b), (e), and (h) show the interface between the ribbon and cell after peeling-off the ribbon, and the failure modes of LT-CF. LT-CF bonded at 110 °C shown in Fig. 3(b) was torn into two pieces and adhered to the ribbon and bus bar; this corresponded to the inadequate cohesive failure mode [10]. This observation implies that the curing of LT-CF was not sufficient to obtain sufficient mechanical bonding strength. However, after peeling-off above 180 °C, most of the parts of LT-CF remained on the cell part; this corresponded to the interface (between ribbon and LT-CF) failure mode [10]. This mode is observed when sufficient adhesion strength is achieved [10].

Fig. 3(c), (f), and (i) show the top-view images of LT-CF, and the inset images clearly show the morphology of the remaining part of LT-CF on the cell after peeling-off of the ribbon. The remaining part of LT-CF had a concave-shaped morphology ([11]). As the bonding temperature increased, the fractured amount of LT-CF decreased. These results agree well with the reaction rate obtained from FT-IR measurements [8]. The reaction rates were 24.3, 91.4, and 93.5 % for 110, 180, and 210 °C, respectively. Depending on the alignment precision degree between the bus bar and LT-CF, the amount of the LT-CF outflow was different along the left and right sides of the bus bar. As shown in the inset images of Fig. 3(c), (f), and (i), the height and width of ridge of the deformed LT-CFs at both end edges did not have a perfect bilateral symmetry. After bonding, 1.2-mm-wide and 25-µm-thick LT-CF beneath the 1.5-mm-wide bus bar was compressed and filled the blank space between the cell and bus bar. Assuming that the degree of precision for the alignment between the bus bar and LT-CF was 100%, the shape of LT-CF was perfectly flat with no ridge formation at both the end edges when the width and thickness of LT-CF were deformed to 1.5 mm and 20 µm, respectively, i.e., a compression rate of 20% in the thickness of LT-CF. Clearly, when the compression rate was greater than 20 %, LT-CF started to flow out. From Fig. 3(c), (f), and (i), the misalignment rate between the bus bar and LT-CF was estimated to be ~1.2 %. Even though misalignment is exhibited in Fig. 3(c) and (f), the width deformation was within 1.5 mm. However, the width was extended to beyond 1.5 mm for LT-CF bonded at 210 °C, as shown in Fig. 3(i). This implies that the compressed thickness and outflow amount of LT-CF increased with the bonding temperature.

The bonding parameters were expressed as V_{BP} to express the dependence of various properties of LT-CF-bonded cells and LT- CF itself on the bonding parameters; V_{BP} was product of temperature (°C), pressure (MPa), and time (h) required to bond one sample. The following parameter ranges were used in this study: temperature, 110–210 °C; pressure, 1–4 MPa; and time, 1–7 s. When one parameter was varied, the other parameters were maintained constant.

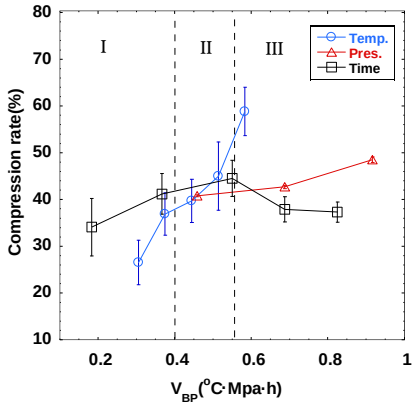

Fig. 4. Compression rate of LT-CFs bonded under various bonding conditions: temperature, 110–210 ℃; pressure, 2–4 MPa; and time, 1–7 s.

The compression rate of LT-CF was evaluated by comparing its thickness before and after compression from the cross-sectional SEM images, after removing the ribbon. For this evaluation, four spots per bus bar were examined, i.e., 12 spots per sample. The values were averaged and the standard deviation was represented as an error bar, as shown in Fig. 4. At the parameter values examined in this study, the compression rate of LT-CF was in the approximate range 20–60 %. As V_{BP} was increased, the compression rate also increased. Among the parameter series, the slope of temperature series (blue open circles) was the largest, indicating that the curing degree of LT-CF was sensitive to temperature. Compared to temperature, the compression rate for pressure series increased only slightly with increasing pressure. Therefore, increasing the bonding temperature rather than pressure is a more effective way for enhancing the compression rate. It should be pointed out that uniformity improved gradually as the bonding time increased; however, the compression rate slightly decreased.

On the basis of the data corresponding to compression rate vs. V_{BP}, the parameter range was divided into three regimes: I. soft regime, II. moderate regime, and III. hard regime; the

ISSN: 2277-9655
Scientific Journal Impact Factor: 3.449
(ISRA), Impact Factor: 2.114

relationship between the compression rate and various other properties will be discussed later. In regime I, temperature was too low to achieve a sufficient curing degree, as shown in Fig. 3(b). Moreover, compression pressure and time were also comparatively low and short, respectively; therefore, sufficient compression was not achieved. On the other hand, in regime III, LT-CF was cured sufficiently enough (>90 %) according to FT-IR results, and compression rates were spread widely from 37.3 to 58.8 %. In regime II, which was intermediate between regimes I and III, V_{BP} ranged from 0.4 to 0.55 °C·MPa·h. In this regime, the values of compression rate ranged from 39.7 to 45.0 %, and reaction rate was in the range 80–90%, approximately.

Since LT-CF that flows out from the region between the ribbon and bus bar after compression contains conductive particles, it is likely to cause degradation in electric as well as mechanical contact properties owing to decrease in the contact volume. Additionally, the shading effect due to LT-CF outflow should also be considered. In Fig. 5, the outflow rate and shading rate, obtained from Fig. 3 and 4, respectively are plotted against the compression rate according to various parameters. The outflow rate of LT-CF was evaluated by subtracting the volume of remaining LT-CF just beneath the 1.5-mm-wide bus bar (obtained from the thickness) from the original volume after compression. The dependence of volume changes in LT-CF on temperature was not considered, and the thickness was assumed to be uniform. The shading rate was obtained by measuring the width of LT-CF flowing out over the width of the bus bar (1.5 mm) from the cross-sectional SEM images shown in Fig. 3(c), (f), and (i). The width was then recalculated to the shaded area in a 6-inch cell. The transmittance of LT-CF was not considered.

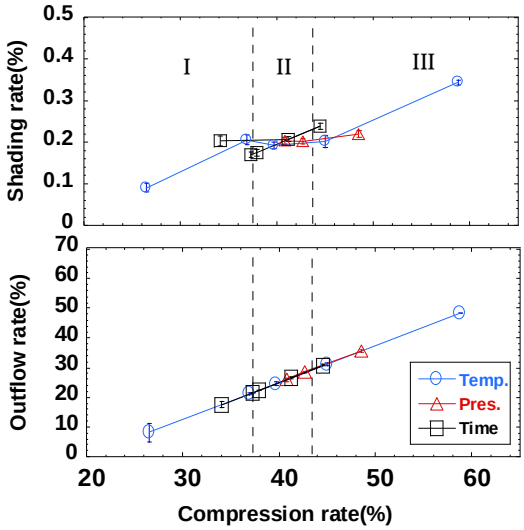

Fig. 5. Dependence of shading rate and outflow rate of LT-CFs bonded under various bonding conditions on compression rate. The Fig. is obtained from Fig. 3 and 4.

The outflow rate increased lineally with the compression rate. As mentioned previously, it is clear that when the compression rate was greater than 20 %, LT-CF started to flow out. However, the shading rate was in the range 0.1–0.35 % for a 6-inch cell corresponding to the parameter ranges examined in this study. It is expected that this shading caused ~0.01–0.03 % power loss in a PV module [11]. This result indicates that the shading effect originating from the outflow of LT-CF after compression on the electrical properties was negligible. The saturation values of the shading rate were observed in the compression rate range from 35 to 45 %; this range was close to regime II. The reason for this result is that LT-CF was likely to be extended along the height direction rather that the width direction in this regime. In contrast, in regime III, LT-CF was extended along the width direction, especially when bonding temperature was increased.

ISSN: 2277-9655
Scientific Journal Impact Factor: 3.449
(ISRA), Impact Factor: 2.114

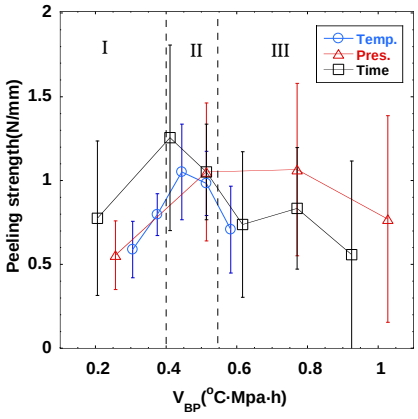

Fig. 6. Peeling strength of LT-CFs bonded under various bonding conditions: temperature, 110–210 ℃; pressure, 1–4 MPa; and time 1–7 s. The values shown are average of three sets of values for 150-mm-long ribbons and were gathered at a rate of 0.7 mm/s for each sample.

The results for the peeling strength of LT-CFs bonded under various bonding conditions showed that the peeling strength increased in regime I and reached its maximum value in regime II, and then gradually decreased in regime III. Generally, epoxy-resin-based LT-CF is sensitive to temperature rather than to other parameters such as pressure and time [12]. As the bonding temperature is increased, the density of cross-linkage increases, resulting in enhanced rheological properties of LT-CF at the interface.

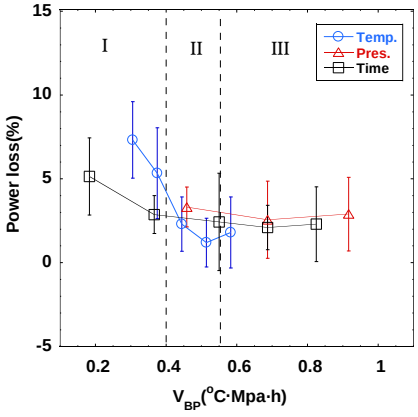

Fig. 7. Power loss in 4.5-Wp solar cells after LT-CF bonding with Pb-free ribbons under various bonding conditions: temperature, 110–210 ℃; pressure, 2–4 MPa; and time, 1–7 s.

However, a too high temperature causes over-curing of CF and decreases adhesion strength [13]. Furthermore, in this study, since the compression rate drastically increased with increasing temperature, as shown in Fig. 4, it decreased the thickness of LT-CF, thereby degrading its adhesive strength. Further, increases in both bonding pressure and time decreased the peeling stress, as shown in regime III. These results presumably account for both over-curing and reduced thickness. According to previous reports, an excessively high bonding pressure may induce compressive stress in LT-CF and internal stress in bonding areas [14].

Fig. 7 shows the power loss in a 4.54-Wp monocrystalline cell after LT-CF bonding with PFR under various bonding conditions. Power loss generally occurs during the bonding process and results in a lower power output. It is likely that the decreased performance of solar strings resulted from the increased series resistance. The power loss was in the range 1.2–7.3 % for the parameter ranges investigated in this study. As V_{BP} increased, power loss decreased steadily but then nearly saturated. This indicates that conditions that result in high compression strength guarantee a good electric contact as well. However, it should be pointed out that the values of power loss in regime III were slightly worse than those in regime II but were still at an acceptable level for production despite the low peeling strength. This result is attributed to the fact that excess compression conditions promoted over-curing and reduced thickness of LT-CF but formed a sufficient pathway made of conductive particles to result in a power loss of only 2–3 %.

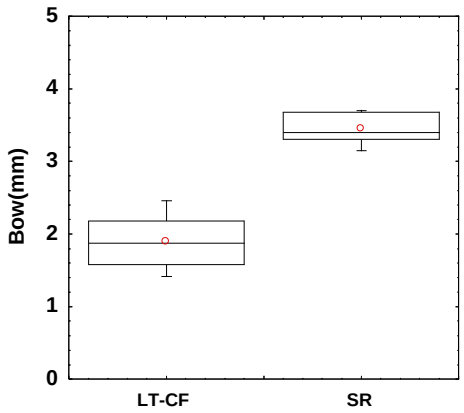

Fig. 8. Bow comparison between PFR/LT-CF-bonded cells assembled for 5 s at 180 ℃ under 2 MPa and SR-bonded cells assembled at 280 ℃. Ten samples were prepared under each condition.

ISSN: 2277-9655
Scientific Journal Impact Factor: 3.449
(ISRA), Impact Factor: 2.114

However, it is expected that samples with weak peeling strength are clearly vulnerable to humidity, thermal and physical shocks, etc., which deteriorates their long-term reliability. The LT-CF bonding parameters of 5 s, 180 °C, and 2 MPa, shown in regime II, yielding a power loss of 1.2% were the best bonding parameter for obtaining a low power loss.

To analyze the effectiveness of the LT-CF process in preventing the thermal stress in comparison to the conventional SR process, the bows of the LT-CF-bonded and conventional SR-bonded cells were compared. Ten cells were assembled under each optimized condition: for 5 s at 180 °C under 2 MPa for the PFR/LT-CF-bonded cells and 280 °C for 2 s for the SR-bonded cells. After bonding, the deflection at the center of the cells was measured. As shown in Fig. 8, the average bow was 3.15 mm for the conventional SR-bonded cells, which agreed well with the bow of 3–5 mm reported in another study [15]. The average bow for the PFR/LT-CF-bonded cells was 1.42 mm, corresponding to a bow suppression of 54.9 %. It has been reported that a low cell thickness and high bonding temperature increase the bow of the cell. Conventional soldering carried out in the temperature range 250–400 °C was observed to result in an average bow of 3–4 mm. This value is equal to that obtained under a residual stress of 100 MPa on the cells [15]. Therefore, it can be concluded that the LT-CF bonding process effectively reduces the thermal stress in comparison to the SR process.

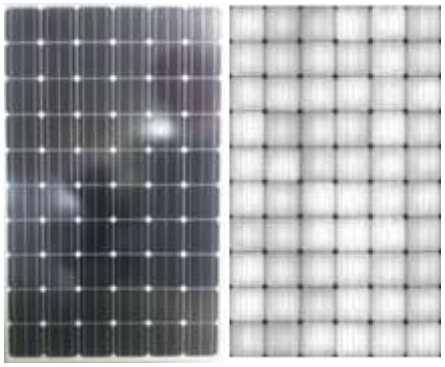

Fig. 9. EL analysis of 250-Wp PV module consisting of LT-CF-bonded cells under the optimized tact time condition of 6 min for a module.

On the basis of the above mentioned results, we fabricated 250-Wp (10 × 6 cells) LT-CF modules under automatically optimized conditions by using the pilot apparatus (ARCF-700). In this process, many parameters related to the apparatus for improving the yield and tact time, such as the positions of ribbon, cell, and LT-CF, and bonding parameters (V_{PB}) were finely tuned through trial and error. Using the optimized apparatus, we were able to assemble a cell per 6 s, i.e., 10 modules per hour. The apparatus optimization process will be discussed in detail elsewhere. First, EL analysis was conducted to confirm the presence of cell cracks induced during the bonding and modulation processes. The EL image displayed in Fig. 6 shows comparatively uniform intensity and no microcracks, indicating that internal voltage and series resistance were uniform in the overall module [16].

Table 2. Summary of photovoltaic characteristics of 250-Wp PV modules consisting of SR-, CF-PFR-, and CF-LCR-bonded cells.

Sample	I_{sc} (A)	V_{oc} (V)	I_{mp} (A)	V_{mp} (V)	P_m (W)	FF (%)	CTM loss (%)
SR1	8.84	38.34	8.34	31.35	261.43	76.97	4.03
SR2	8.81	37.97	8.34	30.89	257.63	77.02	5.42
Average	**8.83**	**38.16**	**8.34**	**31.12**	**259.53**	**77.00**	**4.73**
CF-PFR1	8.87	38.02	8.39	31.13	261.06	77.37	4.16
CF-PFR2	8.88	37.95	8.38	31.01	259.69	77.07	4.66
Average	**8.88**	**37.99**	**8.39**	**31.07**	**260.38**	**77.22**	**4.41**
CF-LCR1	8.99	38.03	8.50	31.07	264.01	77.20	3.08
CF-LCR2	9.00	37.96	8.49	30.95	262.63	76.90	3.58
Average	**9.00**	**38.00**	**8.50**	**31.01**	**263.32**	**77.05**	**3.33**

For the comparison of electrical properties of the LT-CF modules, two different types of modules were fabricated additionally, as summarized in Table 1. The modules were named according to the type of ribbon and bonding process as follows: module SR was fabricated by the conventional soldering process at 250 °C for 2 s using SR, and modules CF-PFR and CF-LCR were fabricated by the same optimized LT-CF process at 180 °C under 2 MPa for 5 s but with different ribbon, PFR, and LCR. The two representative modules for each bonding condition were selected. The I-V characteristics of these modules are shown in Fig. 10, and the detailed parameters are summarized in Table 2. The average power of modules SR, CF-PFR, and LCR was 259.53, 260.38, and 263.32 Wp, corresponding to a cell to module (CTM) loss of 4.73, 4.41, and 3.33 %, respectively. These results indicate that the properties of modules SR and CF-PFR were very similar but those of CF-LCR were approximately 1.5 % higher. From Table 2, it is clear that the LT-CF bonding process provided electrical properties similar to those provided by the conventional soldering process; moreover, LCR (patterned ribbon) improved the electrical properties of the modules. The likely reason

ISSN: 2277-9655
Scientific Journal Impact Factor: 3.449
(ISRA), Impact Factor: 2.114

for this is that the patterned surface effectively enhanced light trapping in the module by increasing the reflection path, resulting in more power generation.

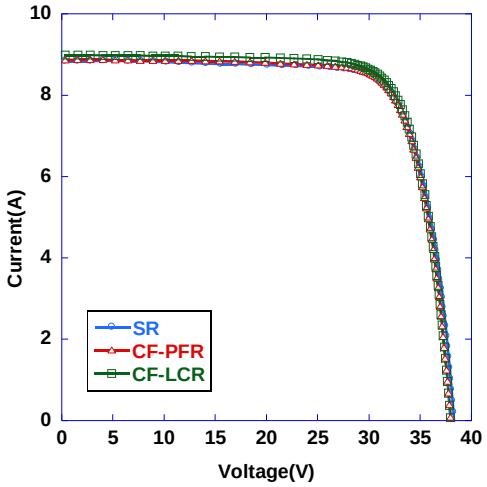

Fig. 10. I-V curve of 250-Wp PV modules consisting of cells bonded using SR (circle), CF-PFR (triangle), and CF-LCR (rectangle). Values for SR1, CF-PFR1, and CF-LCR1 listed in Table II are displayed in this Fig.

Conclusion

In this study, a parameter combining all sample bonding parameters, V_{BP}, was introduced. To the best of our knowledge, such a parameter has not been introduced yet in any other study. The dependence of electrical and mechanical properties such as compression rate (shading rate, outflow rate), peeling strength, and power loss on V_{BF} were analyzed carefully. On the basis of the results obtained, the parameter range was divided into three regimes: I. soft regime, II. moderate regime, and III. hard regime. A suitable regime for strong bonding and low power loss and in which V_{BP} ranged from 0.4 to 0.55 °C·MPa·h, i.e., regime II, was found. The LT-CF-bonded cells in this regime showed a compression rate of 39.7–45.0 %, corresponding to a reaction rate of 80–90 %, peeling strength of ~ 1 N/mm, and power loss of 1.2–3.3 %. It was confirmed that the shading area due to the LT-CF outflow after compression was negligible, and the main reasons causing power loss were the insufficient curing degree of LT-CF in regime I and the reduced thickness in regime III. Even though the samples in regime III showed less power loss than expected from the weak peeling strength, this result needs further observation, focusing on long-time reliability.

From the point of view of industrial PV module production, high temperature and pressure are needed to promote productivity. However, a careful analysis of morphological and chemical exchanges after bonding revealed that these conditions presumably cause excess compression (>40 %), overcuring (>90 %), and reduced thickness of LT-CF, resulting in the degradation of bonding strength. Hence, a suitable shorter bonding time should be examined to achieve LT-CF with properties similar to those of the sample bonded in regime II. For example, if a sample bonded at 210 °C under 2 MPa for 5 s, as existing in regime III, is cured for a reduced time in the range 3.4–4.7 s, it would lie in regime II, according to a simple calculation using V_{BP}. However, as time is shorter, the uniformity reduces. Of course, this assumption needs a modification factor calculated from further experiments to improve accuracy.

From the comparison electrical properties of modules fabricated using SR, CF-PFR, and CF-LCR, it was found that the LT-CF process is comparable to the conventional soldering process for PV module fabrication. Additionally, the LT-CF process is more suitable for obtaining solar cells with steadily decreasing thickness, as revealed by the bow data. Hence, undoubtedly, the LT-CF process is a prime candidate for substituting the conventional soldering process while also being more environmentally friendly

Acknowledgements

This work was partially supported by the New & Renewable Energy Core Technology Program of the Korea Institute of Energy Technology Evaluation and Planning (KETEP), and received a financial grant from the Ministry of Trade, Industry & Energy, Republic of Korea (No. 20113030010070).

This research was partially supported by the Ministry of Trade, Industry & Energy(MOTIE), Korea Institute for Advancement of Technology(KIAT) and Honam Institute for Regional Program Evaluation through the Leading Industry Development for Economic Region(No. R0001246).

References

[1] Liu, J., Lai, Z., Kristiansen, H., Khoo, C., "Overview of conductive adhesive joining technology in electronics packaging applications. In: Adhesive Joining and Coating Technology in Electronics

ISSN: 2277-9655
Scientific Journal Impact Factor: 3.449
(ISRA), Impact Factor: 2.114

Manufacturing", 1998. Proceedings of 3rd International Conference on. IEEE, 1998, pp 1-18.

[2] Ellis B., "Conductive adhesives for electronics packaging" Soldering & Surface Mount Technology , 2000, 12, 1.

[3] Kim Y-S, Lee K, Paik K-W., "Effects of ACF bonding parameters on ACF joint characteristics for high-speed bonding using ultrasonic bonding method.", Components, Packaging and Manufacturing Technology, IEEE Transactions on 2013,; 3.1, pp. 177-182.

[4] Chen, X., Zhang, J., Jiao, C., Liu, Y., "Effects of different bonding parameters on the electrical performance and peeling strengths of ACF interconnection.", Microelectronics Reliability, 2006, 46.5, pp. 774-785.

[5] Uddin, M. A., Alam, M. O., Chan, Y. C., Chan, H. P., "Adhesion strength and contact resistance of flip chip on flex packages—effect of curing degree of anisotropic conductive film.", Microelectronics Reliability 2004, 44.3, pp 505-514.

[6] Funakoshi Y., "Solar battery, method for manufacturing solar battery, method for manufacturing solar cell module, and solar cell module." U.S. Patent Application 12/679,722, 2008.

[7] Abiko Y., "Solar cell module and method for manufacturing solar cell module.", U.S. Patent Application 12/742,144, 2008.

[8] Chan, K. K., Yeung, N. H., Chan, Y. C., Tan, S. C., Lee, K. K., "Microwave curing of anisotropic conductive film: effects of principal parameters on curing situation.", in Electronic Components and Technology Conference. IEEE, 1999, 200, pp 1701-1704.

[9] Islam RA, Chan YC, Ralph B., "Effect of drop impact energy on contact resistance of anisotropic conductive adhesive film joints. ",Journal of Materials Research, 2004, 19.6, pp. 1662-1668.

[10] Chung C-K, Paik K-W., "The effects of the degree of cure of anisotropic conductive films (ACFs) on the contraction stress build-up of ACFs and ACF joints stability for chip-on-flex (COF) applications." in Electronic Components and Technology Conference, 2009. ECTC 2009. 59th. IEEE, 2009; 161-167.

[11] Singh P, Niamat M, Vemuru S. Modeling of random shading effects in solar cells. In: Systems Engineering (ICSEng), 2011 21st International Conference on. IEEE, 2011, pp 86-90.

[12] Lin YC, Zhong J., "A review of the influencing factors on anisotropic conductive adhesives joining technology in electrical applications.", Journal of Materials Science 2008, 43.9, pp 3072-3093.

[13] Wu, Y. P., Alam, M. O., Chan, Y. C., Wu, B. Y., "Dynamic strength of anisotropic conductive joints in flip chip on glass and flip chip on flex packages.", Microelectronics Reliability 2004, 44.2, pp. 295-302.

[14] Yim M-J, Paik K-W., "The contact resistance and reliability of anisotropically conductive film (ACF).", Advanced Packaging, IEEE Transactions on 1999, 22.2, pp. 166-173.

[15] Chen, C. H., Lin, F. M., Hu, H. T., Yeh, F. Y., "Residual stress and bow analysis for silicon solar cell induced by soldering." in International Symposium on Solar Cell Technologies, Taipei, Taiwan, 2008.

[16] Köntges, M., Kunze, I., Kajari-Schröder, S., Breitenmoser, X., Bjørneklett, B., "The risk of power loss in crystalline silicon based photovoltaic modules due to micro-cracks." Solar Energy Materials and Solar Cells , 2011, 95.4, pp. 1131-1137.